JGR Planets

RESEARCH ARTICLE
10.1029/2024JE008687

Effect of Solar Wind and Micrometeoroid Impact on the Lunar Water Cycle: A Molecular Dynamics Study

Anastasis Georgiou[1], Ziyu Huang[2,3], Li Hsia Yeo[4], William Farrell[5,6], Sebastien Verkercke[7], Jesse R. Lewis[1], Chuanfei Dong[3], and Liam S. Morrissey[1]

[1]Faculty of Engineering and Applied Science, Memorial University of Newfoundland, St John's, NL, Canada, [2]Daniel Guggenheim School of Aerospace Engineering, Georgia Institute of Technology, Atlanta, GA, USA, [3]Center for Space Physics and Department of Astronomy, Boston University, Boston, MA, USA, [4]Solar System Exploration Division, NASA Goddard Space Flight Center, Greenbelt, MD, USA, [5]DeepSpace Technology, Inc, Columbia, MD, USA, [6]Space Science Institute, Boulder, CO, USA, [7]LATMOS/CNRS, Université Versailles Saint Quentin, Guyancourt, France

Key Points:

- Water formation is influenced by the location of H in the lunar soil and the impactor angle and size
- Water retention is highly dependent on the H distribution in the lunar grain
- Atomic simulations show the underlying mechanisms of water formation and dissociation following a micrometeoroid impact

Correspondence to:

L. S. Morrissey,
lsm088@mun.ca

Citation:

Georgiou, A., Huang, Z., Yeo, L. H., Farrell, W., Verkercke, S., Lewis, J. R., et al. (2025). Effect of solar wind and micrometeoroid impact on the lunar water cycle: A molecular dynamics study. *Journal of Geophysical Research: Planets*, *130*, e2024JE008687. https://doi.org/10.1029/2024JE008687

Received 26 AUG 2024
Accepted 30 MAR 2025

Abstract We have used molecular dynamics (MD) simulations to better understand the role of solar wind (SW) implanted hydrogen and micrometeoroid impacts on the lunar water cycle. Our simulations consider both the effect of initial hydrogen implantation profile along with the impact characteristics of the micrometeoroid (angle, size). Results show that water formation is strongly influenced by the initial depth location of hydrogen in the lunar soil, along with the impactor's characteristics. When hydrogen is distributed (instead of near surface) we find that nearly all of the water formed after a micrometeoroid impact was retained in the substrate. We also observe an increase in water production when micrometeoroids impact the surface at a normal angle compared to more glancing oblique impacts. In contrast, when micrometeoroids impact the surface of a substrate with near surface hydrogen we observe water loss characteristics and little retention. We also use these models to study the mechanism of water production within the substrate.

Plain Language Summary The presence of OH/H_2O molecules has been detected on the lunar surface. While solar wind implanted protons are a source of the observed OH/H_2O, other processes such as micrometeoroid impacts also affect the lunar water cycle. We present atomistic scale simulations on the effect of solar wind implanted hydrogen and micrometeoroid impact on the lunar water cycle. Results show a clear indication of the effect of both initial hydrogen profile and micrometeoroid impact characteristics (angle, size) on the overall water formation and retention.

1. Introduction

Upcoming lunar exploration missions such as the "Artemis" program will focus their experiments on the lunar south pole where traces of water ice have been detected (Creech et al., 2022). The presence of trapped hydrogen (H) and subsequent water (H_2O) and hydroxyl (OH) in the lunar soil has been well studied and documented in literature during the past couple of decades, with particular focus on its origin on the Moon's surface (Arnold, 1979; Feldman et al., 1998; Zeller et al., 1966). Evidence of OH/H_2O on the Moon's surface has been found by analyzing Chandrayaan-1, Deep Impact, and Cassini flyby data (Clark, 2009; Pieters et al., 2009; Sunshine et al., 2009). Ground truth data observations of lunar surface water were also made by the Lunar CRater Observation and Sensing Satellite (LCROSS) (Colaprete et al., 2010). Observations carried out by the Moon Mineralogy Mapper (M3) team suggested that the existence of such elements could be the result of solar wind (SW) impacting the lunar surface (McCord et al., 2011). The Lunar Trailblazer mission will look to build up on the observed OH/H_2O with the goal to better understand the abundance, form and distribution of water on the Moon (Ehlmann et al., 2022). However, despite the extensive observations of lunar water, research is still needed to better understand the mechanisms underlying its production.

One such mechanism thought to be important in the production of water on airless bodies such as the Moon is the SW (Starukhina, 2006). The SW originates from the Sun's upper atmosphere and contains 95% H^+ with other components such as helium, iron and oxygen present (Ogilvie & Coplan, 1995; Von Steiger et al., 2000). As these SW atoms impact the body, they can both weather the exposed surface and deposit extensive atomic hydrogen throughout the bulk of the mineral. Previous studies have suggested that the implantation of this SW H is an important first step in the formation of subsequent OH/H_2O molecules at the surface through H and O

combination (Clark, 2009; Morrissey et al., 2022; Pieters et al., 2009; Stern et al., 2013). However, SW impacts alone are unlikely to produce enough H_2O to match observed features (Huang et al., 2021a).

As an alternative, thermally activated processes such as recombinative desorption (RD) or associative desorption (AD) can form water molecules on the surface of the Moon through the release of SW created OH (Schörghofer et al., 2021). RD has been discussed in literature (Jones et al., 2024) and has been demonstrated experimentally to occur in the lunar regolith during lunar dayside temperatures due to the abundance of different oxides in the regolith (Jones et al., 2018, 2020). While RD is occurring to some extent at typical dayside temperatures on the lunar surface, H_2O formation via RD peaks at ∼600 K in typical lunar silicates (Gun'ko et al., 1998). This temperature is much greater than the maximum surface temperature on the Moon (∼400 K) (Orlando et al., 2018; J.-P. Williams et al., 2017; Zhu et al., 2019) In addition to RD, more energetic process like micrometeoroid surface impacts could provide short term localized temperature increases via energy deposition that may lead to more efficient water formation (Wu et al., 2017; Zhu et al., 2019). However, research is needed to better quantify the role micrometeoroids play in the water production process.

Experimental and analytical calculations of micrometeoroid impacts have been well documented in the 1970s when lunar samples were returned during the Apollo missions (Gault, 1973; Hartung, 1976; Hörz et al., 1975; Horz et al., 1977; Hutcheon, 1975). Previous research on micrometeoroids impacts on the Moon were conducted to better understand its importance to exosphere formation and surface morphology (Cervone et al., 2022; Cremonese et al., 2013; Sorokin et al., 2020; Nelson et al., 2016). Laboratory experiments conducted by Zhu et al. (2019) using exposed anhydrous olivine $(Mg,Fe)_2SiO_4$ samples showed that water can be formed through energetic heating similar to micrometeoroid impacts on the lunar surface. Li et al. (2015) simulated micrometeoroid impacts at different incident angles studying the ejecta produced by the impact. They found that most of the ejecta is produced during the early stages of the simulation. Cintala (1992) studied the thermal effects of micrometeoroid impact on the surface of the Moon and Mercury and found that the rates of impact melting and vaporization are far greater on Mercury than on the Moon. By assuming an identical micrometeoroid, they found that a factor of 14 more melt and 20 more vapor was produced on Mercury rather than on the Moon (Cintala, 1992). A recent study by Jones et al. (2024) have found that the melting rates are ∼5 larger than those described by Cintala (1992).

While these studies highlight the important role of micrometeoroids in the water production cycle, they report only end result data, without providing insight on the evolution of the surface composition. In addition, macroscopic simulation models and laboratory experiments are unable to simultaneously resolve mechanical collisions and chemical reactions which occur at the atomic scale. In order to better understand the mechanisms underlying water formation and retention, studies at the atomic level need to be conducted. One such option is molecular dynamics (MD) simulations, which have the ability to dynamically capture atomic bonds and molecule formation during different processes. For example, Huang et al. (2021a), used reactive MD to study water production and retention following a micrometeoroid impact on a silicate surface with hydrogen implanted near the surface. Their simulations used a reactive force field (ReaxFF) in order to capture bond breaking and formation of H_2O molecules while testing different impact velocities for a 6 nm micrometeoroid.

Although the results from Huang et al. (2021a) provide valuable insight into micrometeoroid impacts on the lunar surface at the atomic scale, results are limited to H implanted at the near surface (<20 Å in depth) of a lunar grain, similar to those found in the permanently shadowed regions (PSRs). However, previous research on Apollo samples has demonstrated that SW implanted H is instead distributed much deeper in the lunar regolith grains, up to 2,000 Å (Leich et al., 1973). Similarly, MD simulations of SW H implantation on SiO_2 have shown that H can also impinge well below the surface of a grain (Huang et al., 2022; Morrissey et al., 2023). In addition, simulations were limited to a single size micrometeoroid impacting the surface at only the normal direction. While such impacts are possible, a range of micrometeoroid sizes can impact the lunar surface (Cremonese, G. et al., 2013) at different relative incident angles, with 50% of impacts occurring at an angle of less than 45° (Gault & Wedekind, 1978). More research is needed on the effects of impactor size and impact angle. The purpose of this study was to use MD modeling to better understand the effects of different parameters on water formation and retention during micrometeoroid impacts on the lunar surface. We present a parametric study of micrometeoroid impacts by simulating different micrometeoroid sizes, impact angles and H distribution cases tracking H_2O formation and retention. Results can be used to better understand the physics underlying water production on the Moon and other airless bodies.

2. Methodology

2.1. Substrate Setup

The lunar surface is primarily comprised of Si and O atoms which can typically be found as silica (SiO_2) at ∼45 wt.% (McKay et al., 1991). While the surface also consists of various different intermediate silicates such as olivine $(Mg,Fe)_2SiO_4$ and pyroxene (Ca, Mg, Fe)SiO_3 (R. J. Williams & Jadwick, 1980) we modeled the substrate and micrometeoroid as an amorphous SiO_2, following previous simulations and due to limited availability of reactive force fields (Morrissey et al., 2022; Verkercke et al., 2023). The potential selected for the present study was originally parameterized to describe a silica-water system (Fogarty et al., 2010) and was previously used to study the diffusion mechanism of H in amorphous and strained SiO_2 (Georgiou, Yeo, et al., 2024; Morrissey et al., 2022; Sheikholeslam et al., 2016). Simulations were carried out using Large-scale Atomic/Molecular Massively Parallel Simulation (LAMMPS) package (Plimpton & Thompson, 2012). An amorphous substrate was chosen to represent the weathered near surface rims formed at the Moon due to prolonged exposure (Bibring et al., 1972; Poppe et al., 2018). A $433 \times 433 \times 290$ Å^3 substrate containing 1152000 SiO_2 molecules was created that represents the outer surface of a lunar grain. The substrate volume was approximately 3 times larger than those used by Huang et al. (2021a), in order to account for the possible effect of high temperature waves interacting with the periodic walls of the substrate. The amorphous silica substrate was created following the melting recipe used by Morrissey et al. (2022). The substrate was then equilibrated at a temperature of 100 K using a barostat and thermostat ensemble for a total of 20 ps. The simulation temperature was chosen to represent the expected values found in PSRs as well as following previous similar simulations (Huang et al., 2021a, 2021b; Paige et al., 2010). Given the high energy found for micrometeoroid impacts, we do not expect the initial substrate temperature to have a significant effect on water production. The density of the equilibrated substrate was 2.1 g/cm^3, agreeing well with previous experimental results (2.2 g/cm^3 (Haynes, 2016)) and validating the approach. The simulation domain was then extended in the z-direction to expose a free surface to vacuum. The final simulation box was $433 \times 433 \times 1220$ Å^3 with periodic boundary conditions applied in the x- and y-direction. The domain in the z-direction was set as fixed with its height being sufficiently large enough to capture any ejected molecules. The bottom of the substrate was fixed in space so that the atoms didn't shift during impact.

2.2. Hydrogen Placement

After developing the silica substrate, H atoms were then placed as interstitial atoms following two different distributions prior to impacting with a micrometeoroid. While the overall H concentrations present in this study may be inconsistent with measurements in sub-20 micron lunar grains (Bustin et al., 1984), our aim was to study how water formation is affected by the different parameters studied. Thus we decided that the concentration of H was sufficient to capture the effect of each parameter.

Figure 1 shows the depth profiles of H for the two cases considered. First, to generate a SW implanted distribution of H (Figure 1a) we used the distribution reported by Morrissey et al. (2023) in their best practice study on SW simulations using binary collision approximation (BCA) modeling. These simulations were based on H impacting a silicate target with a distribution of impact energies peaking at 1 keV and a cosine distribution of incidence angles. See Morrissey et al. (2023) for more detail on these BCA simulations. Following this distribution, 34,000 H atoms (1% of total number of atoms) were placed throughout the silica substrate (Figure 1a).

Following previous research (Huang et al., 2021a, 2021b), we also placed ∼30,000 H atoms (0.9% of the total number of atoms) in a near surface region (Figure 1b) of the substrate, in order to observe the effect of H deposition location on the overall H_2O retention. The silica substrate dimensions remained as previously described. For both cases, once hydrogen was placed in the substrate it was minimized to allow it to reach its preferential low energy sites.

2.3. Micrometeoroid Impact and Post-Processing

Finally, an SiO_2 micrometeoroid was placed at 6 nm above the surface of the substrate, far enough so that no interactions were present between the impactor and target surface. Micrometeoroids with a diameter of 3, 6, and 9 nm were simulated impacting the silica substrate. For the 3 nm micrometeoroid case, which had a lower net

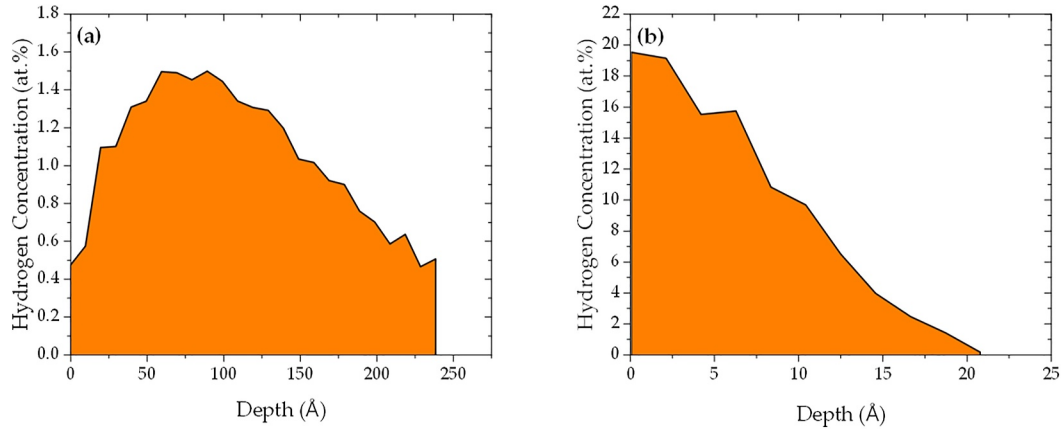

Figure 1. Distribution of hydrogen (a) throughout the substrate and (b) at the near surface of the substrate.

impact energy, the substrate size was reduced to $217 \times 217 \times 250$ Å^3 in order to save on computational resources. The H concentration and distribution were kept consistent with the larger impactor sizes (Figure 1). For all cases an impactor velocity of 12 km/s was selected, the most common velocity for micrometeoroid impacts on the lunar surface (Cintala, 1992). In order to capture the effect of incidence angle, all distributed H cases were simulated at a 90° and 30° impact angle relative to the surface, while near surface H cases were simulated at a 30° angle only (due to previous availability of normal incidence angle cases from MD simulations). The selected oblique angles were chosen based on previously conducted impact simulations and experiments (Gault & Wedekind, 1978; Li et al., 2015). The total simulation time was set to 100 ps, allowing ample time for energy to dissipate for the most extreme case of a 9 nm micrometeoroid. While we note that micrometeoroids at the Moon typically range from microns to a few centimeters (Hörz et al., 1975), the computational limitations of MD only allows for nanometer size impactors.

Because ReaxFF allows for bond order dependent quantities to change every timestep, a smaller timestep than other MD methods and potentials is often required (Chenoweth et al., 2008). A timestep of 0.1 fs was used for all simulations. This follows previous MD simulations for silica impacts (Huang et al., 2021a; qi Shen et al., 2019; Rahnamoun & van Duin, 2016) and suggestions by Chenoweth et al. (2008) who found that a 0.1 fs timestep allows for collision and reactions to occur smoothly for high temperature (2,500 K) MD ReaxFF simulations. To identify the water molecules during the simulation, an Open Visualization Tool ((OVITO) (Stukowski, 2009)) cluster analysis was performed based on a cutoff distance of 1.2 Å as described by Jia et al. (2022). OVITO is widely used in MD simulations for visualization and post-processing of results. The cluster analysis decomposes the particles into clusters based on a neighboring criterion such as the cutoff distance. This method was verified by using the LAMMPS reaxff/species tool, which uses bond-order values to determine chemical bonds. Water molecules detected 50 Å above the surface were considered ejected whereas any that remained in the substrate were considered local on the substrate.

3. Results and Discussion

3.1. Initial Hydrogen Placement

The species found in the substrate after the initial H implantation, prior to micrometeoroid impacts, can be seen in Table 1. For all cases the H has formed different compounds within the substrate, agreeing with previous MD simulations (Huang et al., 2022). For both H depth profiles the most common species was OH, indicating that H preferred to bond with O. Previous research of H implantation in silicates found that ∼90% of the implanted H formed OH bonds (Schaible & Baragiola, 2014). The number of pre-existing water molecules was highly dependent on whether the H was concentrated near surface or distributed throughout. For a SW distribution of H only 0.4%–0.6% of the total implanted H formed a water molecule. In contrast, when the H was instead focused in the near surface the pre-existing water increased to 16%–22%. When H is focused in a smaller region there is an increased probability that an H atom will find an OH pair, forming H_2O. Therefore, the depth profile of implanted H has a significant effect on the number of pre-existing species formed in the substrate. When H is distributed as

Table 1
Total Number of Species Formed During the Implantation Stage

	Substrate volume (nm^3)	N_{H_2O}	N_{H_2}	N_{OH}	N_H
Distributed H	54371.8	71 (0.4%)	108 (0.6%)	23,769 (70%)	9,749 (29%)
Near Surface H		3,305 (22%)	292 (2%)	18,819 (63%)	3,851 (13%)
Distributed H	11772.3	16 (0.6%)	13 (0.4%)	6,473 (79%)	1,684 (20%)
Near Surface H		636 (16%)	181 (5%)	5,874 (75%)	274 (4%)

per SW implantation, the number of water molecules is low, supporting previous conclusions by Orlando et al. (2018) that SW deposition alone is likely an insufficient source to explain observed lunar water.

3.2. Micrometeoroid Impact and Crater Characteristics

Figure 2 shows a cross-section of the substrate colored by the temperature at different simulation times post impact for the 9 nm micrometeoroid case. Similar to previous silica impact simulations (Samela & Nordlund, 2010), it can be seen that an impact crater is formed during normal impacts which was also present during the oblique impact angle cases. Energy shock waves are clearly visible at 4 ps (3 ps after impact), where the crater reaches its maximum depth (Figure 2a). Crater and impactor results can be seen in Table 2, where D_a is the diameter and p is the depth of the crater respectively. Our simulations show that oblique impact cases eject more micrometeoroid fragments than normal impacts, with up to 41% of the 9 nm micrometeoroid material ejected from the surface (Table 2). The remaining material remained at the crater wall. Interestingly, the diameter to depth ratio measured in our simulations increases for a more oblique angle (Table 2), which is opposite to what Gault (1973) found using empirical equations of impacts for projectiles of 10^{-3}cm in size.

As expected, the thermal propagation rate is faster for higher energy impacts (of 9 nm) and reaches higher temperatures at the depth of the substrate for 90° impacts (Figure 2a). However, as can be seen in Figure 2, even for the highest energy cases the heat still dissipates with time, suggesting that shock wave propagation/reflection is not an issue and that the simulated substrate size was sufficient. While Benna et al. (2019) suggest that during high energy meteoroid impacts the energy decays more rapidly, we find that at the nanoscale the heat dissipates at a much higher rate at lower impact energies, with atoms exhibiting higher temperatures for the larger impactor cases. Energy dissipation observed may also be a result of the highly energetic atoms leaving the system during the first few picoseconds after impact.

3.3. Water Formation

3.3.1. Distributed H

Table 2 presents our MD simulation results of water formation during micrometeoroid impacts with distributed H. The distributed case represents the expected depth profile of SW implanted H as reported in previous studies (Leich et al., 1973; Morrissey et al., 2022). The H_2O ratios represent the fraction of H_2O molecules remaining in the substrate at the end of the simulation relative to the initial count of H_2O molecules. During impacts on substrates with distributed H we find that almost all produced H_2O is retained in the substrate. Only a 6 nm

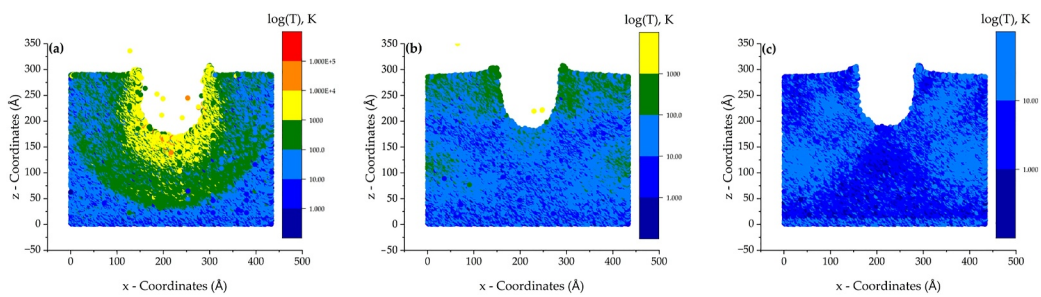

Figure 2. Cross section of substrate at (a) 4 ps (b) 20 ps (c) 65 ps of the simulation for a 9 nm micrometeoroid at normal impact.

Table 2
Simulation Results Following Impact for the Distributed and Near Surface Hydrogen Cases as a Function of Impactor

d (nm)	Mass (g)	Energy (J)	Angle (°)	$N^{H_2O}_{final}/N^{H_2O}_{initial}$ Distributed	$N^{H_2O}_{final}/N^{H_2O}_{initial}$ Near surface	D_a/p	$M^{impactor}_{ejected}$ (g)
3	3.05×10^{-20}	2.2×10^{-15}	30	1.07	0.91	3.3	5.8×10^{-21} (19%)
			90	1.07	–	1.21	6.1×10^{-22} (2%)
6	2.39×10^{-19}	1.8×10^{-14}	30	0.94	0.89	2.59	9.08×10^{-20} (38%)
			90	1.15	1.11[a]	1.09	2.39×10^{-20} (1%)
9	8.05×10^{-19}	5.8×10^{-14}	30	1.05	0.80	2.43	3.30×10^{-19} (41%)
			90	1.19	–	1.2	5.8×10^{-21} (0.7%)

[a]Values by Huang et al. (2021a).

micrometeoroid at normal impact produced ejected H_2O, just one molecule (7% of the total water molecules created). We also see a distinct difference in water production when changing both the impactor size and incident angle for 6 and 9 nm impactors. For such cases normal impacts produce more overall H_2O than oblique impacts. For example, in the case of a 6 nm impactor a normal impact creates a factor of 1.21 more water molecules than an oblique impact. We suggest that the source of this difference is the depth region in which the high temperature spikes are generated during impacts, which stay local to around 150 Å in depth. The observed water loss during a 6 nm oblique impact case is due to H_2O dissociation that takes place within the substrate. The diameter-to-depth ratio observed in Table 2 is also an indication of the effect of an oblique impact that penetrates just a few tens of angstroms. Water molecules created during the implantation stage at a depth of <100 Å are now destroyed, and the absence of a high temperature distribution means atoms deeper in the substrate do not reach a sufficient temperature to form new H_2O molecules. When considering a 3 nm impactor, we observe the same water yield in both oblique and normal impacts, with very little water produced and retained. Therefore, at these smaller sizes insufficient energy is being supplied at depth to have a significant effect on water production.

It should be noted that the impactor sizes simulated are unable to reach the expected peak concentration of hydrogen on the Moon, located at a depth of 100 nm (Leich et al., 1973). Cintala (1992) found that projectiles with a mass of 10^{-6} g produce the most impact melt and vaporization. Such impactors can only provide more water if the lunar soil has no desiccated layer. Benna et al. (2019) suggest that micrometeoroids with a mass of greater than 0.15 g can pierce through the desiccated layer of 7–9 cm, contributing significantly more to the lunar water cycle. As our simulations indicate that the water production increases with an increase in micrometeoroid size, we expect a more substantial increase in water production when considering micrometeoroid sizes described in both Cintala (1992) and Benna et al. (2019).

3.3.2. Near Surface H

To better understand the effect of initial H implantation on water production we also performed impact simulations on an SiO_2 substrate with H saturated at the near surface (<20 Å in depth). Tables 2 and 3 present the results of H_2O retention and ejection different micrometeoroid sizes at an impact angle of 30°. Normal impacts were not simulated as they were already completed previously by Huang et al. (2021a) In contrast to our MD simulations of distributed H which had a net increase in total water formation, when H is deposited near the surface we show a net loss in water production for oblique impacts. This agrees well with previous studies that reported that the lunar surface is in a net water loss regime due to micrometeoroid bombardment (Benna et al., 2019; Pabari et al., 2020; Pokorny et al., 2021; Schörghofer et al., 2021). While the fraction of water retained within the substrate decreases, there is a higher count of ejected water molecules than the distributed case. Therefore, changing the initial depth profile of the H has a significant effect on the new water production rate, along with behavior of the water that is produced.

Table 3
Number of Ejected Species During 30° Impacts on Near Surface Hydrogen Cases

d (nm)	$N^{H_2O}_{ejected}$	$N^{H}_{ejected}$	$N^{H_2}_{ejected}$	$N^{OH}_{ejected}$
3	10	10	4	31
6	72	116	13	237
9	135	73	21	707

As also seen for the distributed case, the impactor size and angle also affects the overall water retention. We observe a more significant decrease in H_2O

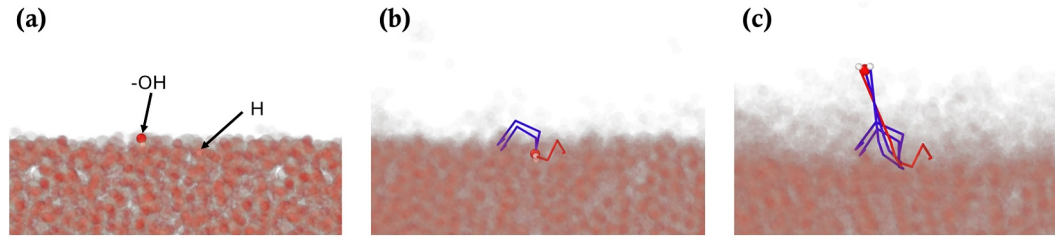

Figure 3. H_2O formation and ejection process where the blue lines represent OH molecule path and red line represents the H atom path. (a) Initial position (b) H_2O formation (c) H_2O ejection.

concentration when increasing the impactor size for near surface cases (Table 2). A larger impactor will produce more ejected molecules resulting in less water retained within the substrate. Previous work by Huang et al. (2021a) for normal impacts onto an SiO_2 substrate with H deposited in the near surface region instead found an increase of retained water production of 11% relative to the initial concentration, while they also reported that 17% of the water escaped from the substrate after impact. Therefore, whether a surface is in a net H_2O loss or production regime depends both on the initial depth profile of the H and the local incidence angle of the impactor. Those surfaces with H initially deposited at depth are more likely to retain the produced water. Benna et al. (2019) have suggested that micrometeoroids smaller than 0.15 g have minimal contribution to the lunar exosphere if a desiccated layer is present. Our results predict only a small fraction of produced water being ejected, supporting this conclusion.

Due to the nature of the concentration of H on the surface of the substrate we also observe an abundance of different volatiles such as H, H_2 and OH being ejected compared to distributed H cases (Table 3). As suggested by previous research (Hurley et al., 2017) and results gathered during our simulations, micrometeoroid impacts are an insufficient source for the H_2 in the lunar exosphere observed by the Lyman Alpha Mapping Project (LAMP). We also observe atomic hydrogen and hydroxyl molecules being ejected during the impact process. The Neutral Mass Spectrometer (NMS) instrument onboard the Lunar Atmosphere and Dust Environment Explorer (LADEE) spacecraft took 743 measurements of exospheric water, of which the most intense can be associated with known meteoric events on the lunar surface (Benna et al., 2014). Based on our findings in Table 3 that OH is more readily ejected than H_2O, it could be possible that the measured water content from the NMS instrument contains high levels of OH since the NMS cannot distinguish whether the measured water is H_2O or OH (Benna et al., 2019).

3.4. H_2O Formation and Dissociation Mechanism

3.4.1. H_2O Formation

In addition to being able to quantify the water production and retention during micrometeoroid impacts, MD simulations can be used to probe the atomic scale mechanisms underlying H_2O formation during impacts. Previous research has suggested that recombinative desorption is a possible mechanism of water formation on the lunar surface (Schörghofer et al., 2021). However, such a process is activated at temperatures above the lunar maximum of 400 K (Orlando et al., 2018; J.-P. Williams et al., 2017; Zhu et al., 2019). We show that the energy and temperature provided to the silica substrate during micrometeorite impacts can provide the necessary conditions in the short-term to activate the RD process. Figure 3 shows the RD process occurring within the first 10 ps of the simulation at the surface of our hydroxylated SiO_2 substrate. The desorbed molecule was observed to be less than 10 Å away from the impact site where the temperature reached more than 1,000 K. Initially, the H_2O molecule is split into OH and H (Figure 3a). As the impact occurs and the surface temperature increases, both OH and H diffuse along the surface (Figure 3b) until they combine and eventually desorb from the surface (Figure 3c). Hydroxyls are bound to the surface at a higher binding energy than water molecules, and will diffuse on the surface until they form a water molecule which decreases the binding energy and allows for desorption (Hibbitts et al., 2011). Morrissey et al. (2022) used MD to study H diffusion in the bulk amorphous SiO_2 and at 100–700 K and observed only H atoms diffusing from one oxygen atom to another. They suggested that OH diffusion was unlikely at expected lunar temperatures and that even H diffusion was limited. In contrast, present results show that the short-term local temperature spikes found during micrometeorite impacts increase diffusion drastically and unlock the potential for both the OH and H to move along the surface until recombinative desorption occurs.

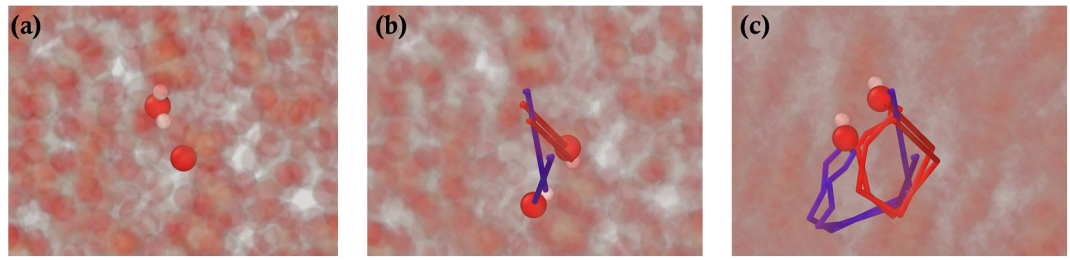

Figure 4. H_2O bond breakage process where the blue lines represent the path of the OH molecule created through H gain while the red lines represent the path of the OH created through H loss. (a) Initial position (b) H_2O breakage and OH formation (c) OH retention.

3.4.2. H_2O Dissociation

While micrometeoroid impacts can provide sufficient energy to form H_2O molecules, they can also lead to H_2O bond breakage (Figure 4) and the loss of water. Two different mechanisms of H_2O dissociation were present in our simulations that agree with previously observed H_2O bond breakage at high temperatures (Baykara, 2004; Morrissey et al., 2022). Both follow the general form of water thermolysis $H_2O \rightarrow H + OH$ but in one case the hydrogen does not bond with a nearby atom whereas in the other the hydrogen bonds to an oxygen forming OH. The latter has been previously described by Morrissey et al. (2022) using MD simulations of hydrogen diffusion at high temperatures where hydrogen atoms can jump from one oxygen to another. This is also clearly depicted in Figure 4 were a hydrogen atom splits from the H_2O molecule combining with a neighboring oxygen atom. This process takes place within the first 10 ps where the energy and temperature is high enough (>2,500 K) to cause water thermolysis. We observe H_2O dissociation throughout the SiO_2 substrate with a more distinct H_2O concentration decrease at the near surface regions (<40 Å), where the energy and subsequent temperature is higher.

4. Conclusions

We have used MD simulations to carry out a parametric study to better understand the different factors affecting water formation and retention on the lunar surface during micrometeoroid impacts. Simulations combine both the effect of initial H implantation profile along with the impact characteristics of the micrometeoroid (angle, size). Results show a clear indication on how water formation can be influenced by the location of hydrogen in lunar soil, the impactor angle, and size. When the hydrogen is distributed throughout the grain we observe both a net increase and net loss of water depending on impact size and angle. In addition, almost all water produced in these cases is retained in the substrate. Water loss characteristics were mainly present when the hydrogen was saturated at the near surface of the substrate (<20 Å). Simulations of a smaller size micrometeoroid (3 nm) displayed the same behavior when simulating an oblique and normal impact for distributed H cases. When studying the near surface H deposition of the same size we found that water is lost both due to local temperature increase and ejection at a similar rate with the other simulations. While the 3 nm micrometeoroid did not show a difference during normal and oblique impacts on distributed H cases, it demonstrated the importance of H distribution even at small energies. We have also presented an atomistic scale view of the water formation and dissociation mechanisms during hypervelocity impacts.

Computational resources limit us to micrometeoroid sizes of only a few nanometers and only a single velocity. When simulating larger impactors at higher velocities and impact energies, a much larger substrate might be needed to account for the effect of high thermal shock waves reaching the "walls" of the simulation box. However, we expect that much larger micrometeoroids can reach a more significant depth. Such sizes could also potentially cause more water loss due to emission on distributed hydrogen cases due the larger energy deposition. In addition, we have tested just two different impact angles, but parametric studies need to be conducted using impacts angles of more than 30° to better understand the water formation during different incident angles. Future studies can also focus on more complex lunar regolith structures such as olivine $(Mg,Fe)_2SiO_4$ and pyroxene (Ca, Mg, Fe)SiO_3 and look beyond the scope of water formation, tracking other ejected species during impact.

Data Availability Statement

The data used to produce the graphs present are available at Georgiou, Ziyu, et al. (2024).

Acknowledgments
This work is supported by SSERVI-CLEVER (NNH22ZDA020C/80NSSC23M022) and the International Space Science Institute (ISSI) in Bern, through ISSI International Team project #24-616 "Multi-scale Understanding of Surface-Exosphere Connections (MUSEC)". A.G. and L.M. were supported in part by the NSERC Discovery Grant and the CSA Research Opportunities in Space Sciences program awards. WFM gratefully acknowledges funding from the SSERVI/CLEVER team at Georgia Tech (Grant 80NSSC23M022). Z.H. and C.D. were supported, in part, by NASA Grant 80NSSC23K0894.

References

Arnold, J. R. (1979). Ice in the lunar polar regions. *Journal of Geophysical Research*, *84*(B10), 5659–5668. https://doi.org/10.1029/JB084iB10p05659

Baykara, S. (2004). Experimental solar water thermolysis. *International Journal of Hydrogen Energy*, *29*(14), 1459–1469. https://doi.org/10.1016/j.ijhydene.2004.02.011

Benna, M., Hurley, D. M., Stubbs, T. J., Mahaffy, P. R., & Elphic, R. C. (2019). Lunar soil hydration constrained by exospheric water liberated by meteoroid impacts. *Nature Geoscience*, *12*, 333–338. https://doi.org/10.1038/s41561-019-0345-3

Benna, M., Mahaffy, P. R., Hurley, D., Stubbs, T. J., Hodges, J. R. R., & Elphic, R. C. (2014). LADEE NMS observations of sporadic water and carbon dioxide signatures in the lunar exosphere. In *Agu fall meeting abstracts* (Vol. 2014, p. P21F-02).

Bibring, J. P., Duraud, J. P., Durrieu, L., Jouret, C., Maurette, M., & Meunier, R. (1972). Ultrathin amorphous coatings on lunar dust grains. *Science*, *175*(4023), 753–755. https://doi.org/10.1126/science.175.4023.753

Bustin, R., Kotra, R. K., Gibson, E. K., Nace, G. A., & McKay, D. S. (1984). Hydrogen abundances in lunar soils. In *Lunar and Planetary Science Conference* (pp. 112–113).

Cervone, A., Topputo, F., Speretta, S., Menicucci, A., Turan, E., Di Lizia, P., et al. (2022). Lumio: A cubesat for observing and characterizing micro-meteoroid impacts on the lunar far side. *Acta Astronautica*, *195*, 309–317. https://doi.org/10.1016/j.actaastro.2022.03.032

Chenoweth, K., van Duin, A. C. T., & Goddard, W. A. (2008). Reaxff reactive force field for molecular dynamics simulations of hydrocarbon oxidation. *The Journal of Physical Chemistry A*, *112*(5), 1040–1053. (PMID: 18197648). https://doi.org/10.1021/jp709896w

Cintala, M. J. (1992). Impact-induced thermal effects in the lunar and mercurian regoliths. *Journal of Geophysical Research*, *97*(E1), 947–973. https://doi.org/10.1029/91JE02207

Clark, R. N. (2009). Detection of adsorbed water and hydroxyl on the Moon. *Science*, *326*(5952), 562–564. https://doi.org/10.1126/science.1178105

Colaprete, A., Schultz, P., Heldmann, J., Wooden, D., Shirley, M., Ennico, K., et al. (2010). Detection of water in the LCROSS ejecta plume. *Science*, *330*(6003), 463–468. https://doi.org/10.1126/science.1186986

Creech, S., Guidi, J., & Elburn, D. (2022). Artemis: An Overview of NASA's Activities to Return Humans to the Moon. In *IEEE Aerospace Conference 2022*.

Cremonese, G., Borin, P., Lucchetti, A., Marzari, F., & Bruno, M. (2013). Micrometeoroids flux on the Moon. *Astronomy & Astrophysics*, *551*, A27. https://doi.org/10.1051/0004-6361/201220541

Ehlmann, B. L., Klima, R. L., Seybold, C. C., Klesh, A. T., Au, M. H., Bender, H. A., et al. (2022). NASA'S lunar trailblazer mission: A pioneering small satellite for lunar water and lunar geology. In *2022 IEEE Aerospace Conference (AERO)* (pp. 1–14). https://doi.org/10.1109/AERO53065.2022.9843663

Feldman, W. C., Maurice, S., Binder, A. B., Barraclough, B. L., Elphic, R. C., & Lawrence, D. J. (1998). Fluxes of fast and epithermal neutrons from lunar prospector: Evidence for water ice at the lunar poles. *Science*, *281*(5382), 1496–1500. https://doi.org/10.1126/science.281.5382.1496

Fogarty, J. C., Aktulga, H. M., Grama, A. Y., Van Duin, A. C., & Pandit, S. A. (2010). A reactive molecular dynamics simulation of the silica-water interface. *Journal of Chemical Physics*, *132*(17). https://doi.org/10.1063/1.3407433/951992

Gault, D. E. (1973). Displaced mass, depth, diameter, and effects of oblique trajectories for impact craters formed in dense crystalline rocks. *The Moon*, *6*(1–2), 32–44. https://doi.org/10.1007/BF02630651

Gault, D. E., & Wedekind, J. A. (1978). Experimental studies of oblique impact. In *Lunar and Planetary Science Conference Proceedings* (Vol. 3, pp. 3843–3875).

Georgiou, A. P., Ziyu, H., Yeo, L. H., Farrell, W., Verkercke, S., Lewis, J. R., et al. (2024). Effect of solar wind and micrometeoroid impact on effect of solar wind and micrometeoroid impact on the lunar water cycle: A molecular dynamics study [Dataset]. https://doi.org/10.5281/zenodo.13328936

Georgiou, A. P., Yeo, L. H., Morrissey, L. S., McLain, J. L., Lewis, J. R., & Tucker, O. J. (2024). Understanding experimental observations of hydrogen desorption via atomistic modelling. In *LPI Contributions* (Vol. 3040, p. 1161).

Gun'ko, V., Zarko, V., Chuikov, B., Dudnik, V., Ptushinskii, Y., Voronin, E., et al. (1998). Temperature-programmed desorption of water from fumed silica, silica/titania, and silica/alumina. *International Journal of Mass Spectrometry and Ion Processes*, *172*(3), 161–179. https://doi.org/10.1016/S0168-1176(97)00269-3

Hartung, J. B. (1976). Lunar microcraters and interplanetary dust fluxes. In H. Elsaesser & H. Fechtig (Eds.), *Interplanetary dust and zodiacal light* (Vol. 48, pp. 207–226). https://doi.org/10.1007/3-540-07615-8_483

Haynes, W. M. (2016). *CRC handbook of chemistry and physics*. CRC Press.

Hibbitts, C., Grieves, G., Poston, M., Dyar, M., Alexandrov, A., Johnson, M., & Orlando, T. (2011). Thermal stability of water and hydroxyl on the surface of the moon from temperature-programmed desorption measurements of lunar analog materials. *Icarus*, *213*(1), 64–72. https://doi.org/10.1016/j.icarus.2011.02.015

Hörz, F., Brownlee, D., Fechtig, H., Hartung, J., Morrison, D., Neukum, G., et al. (1975). Lunar microcraters: Implications for the micrometeoroid complex. *Planetary and Space Science*, *23*(1), 151–172. https://doi.org/10.1016/0032-0633(75)90076-8

Horz, F., Morrison, D., Gault, D., Oberbeck, V., Quaide, W., Vedder, J., et al. (1977). *The micrometeoroid complex and evolution of the lunar regolith* (Vol. 370, pp. 605–635). NASA Special Publication.

Huang, Z., Nomura, K.-I., Morrissey, L. S., & Wang, J. (2022). Molecular dynamics simulation of solar wind implantation in the permanently shadowed regions on the lunar surface. *Geophysical Research Letters*, *49*(18), e2022GL099333. https://doi.org/10.1029/2022GL099333

Huang, Z., Nomura, K.-I., & Wang, J. (2021a). Molecular dynamics simulations of water formation and retention by micrometeoroid impact on lunar surface. *Geophysical Research Letters*, *48*(15), e2021GL093509. https://doi.org/10.1029/2021GL093509

Huang, Z., Nomura, K. N., & Wang, J. W. (2021b). Modeling solar wind implantation and its contributions to volatile formation on lunar surface. In *52nd Lunar and Planetary Science Conference* (p. 1798).

Hurley, D. M., Cook, J. C., Retherford, K. D., Greathouse, T., Gladstone, G. R., Mandt, K., et al. (2017). Contributions of solar wind and micrometeoroids to molecular hydrogen in the lunar exosphere. *Icarus*, *283*, 31–37. https://doi.org/10.1016/j.icarus.2016.04.019

Hutcheon, I. D. (1975). Microcraters in Oriented Vugs-Evidence for an Anisotropy in the micrometeoroid flux. In *Lunar and Planetary Science Conference* (Vol. 6, p. 420).

Jia, J., Wu, D., Ren, Y., & Lin, J. (2022). Nanoarchitectonics of Illite-based materials: Effect of metal oxides intercalation on the mechanical properties. *Nanomaterials*, *12*(6), 997. https://doi.org/10.3390/NANO12060997

Jones, B. M., Aleksandrov, A., Dyar, M. D., Hibbitts, C. A., & Orlando, T. M. (2020). Investigation of water interactions with Apollo lunar regolith grains. *Journal of Geophysical Research: Planets*, *125*(6), e2019JE006147. https://doi.org/10.1029/2019JE006147

Jones, B. M., Aleksandrov, A., Hibbitts, K., Dyar, M. D., & Orlando, T. M. (2018). Solar wind-induced water cycle on the Moon. *Geophysical Research Letters*, *45*(20), 10959–10967. https://doi.org/10.1029/2018GL080008

Jones, B. M., Carrillo-Sánchez, J. D., Janches, D., Sarantos, M., & Orlando, T. M. (2024). Water generation on the Moon from solar wind and meteoroid impacts. *The Planetary Science Journal*, *5*(8), 171. https://doi.org/10.3847/PSJ/ad5542

Leich, D., Tombrello, T., & Burnett, D. (1973). The depth distribution of hydrogen in lunar materials. *Earth and Planetary Science Letters*, *19*(3), 305–314. https://doi.org/10.1016/0012-821X(73)90080-0

Li, Y., Srama, R., Wu, Y., & Grün, E. (2015). Modeling the detection of impact ejecta on the lunar surface. *Planetary and Space Science*, *119*, 185–193. https://doi.org/10.1016/j.pss.2015.09.019

McCord, T. B., Taylor, L. A., Combe, J. P., Kramer, G., Pieters, C. M., Sunshine, J. M., & Clark, R. N. (2011). Sources and physical processes responsible for OH/H_2O in the lunar soil as revealed by the Moon Mineralogy Mapper (M3). *Journal of Geophysical Research*, *116*(E6), E00G05. https://doi.org/10.1029/2010JE003711

McKay, D. S., Heiken, G., Basu, A., Blanford, G., Simon, S., Reedy, R., et al. (1991). The lunar regolith. In G. H. Heiken, D. T. Vaniman, & B. M. French (Eds.), *Lunar sourcebook, a user's guide to the Moon* (pp. 285–356).

Morrissey, L. S., Pratt, D., Farrell, W., Tucker, O., Nakhla, S., & Killen, R. (2022). Simulating the diffusion of hydrogen in amorphous silicates: A "jumping" migration process and its implications for solar wind implanted lunar volatiles. *Icarus*, *379*, 114979. https://doi.org/10.1016/j.icarus.2022.114979

Morrissey, L. S., Schaible, M. J., Tucker, O. J., Szabo, P. S., Bacon, G., Killen, R. M., & Savin, D. W. (2023). Establishing a best practice for sdtrimsp simulations of solar wind ion sputtering. *The Planetary Science Journal*, *4*(4), 67. https://doi.org/10.3847/PSJ/acc587

Nelson, A. O., Dee, R., Gudipati, M. S., Horányi, M., James, D., Kempf, S., et al. (2016). New experimental capability to investigate the hypervelocity micrometeoroid bombardment of cryogenic surfaces. *Review of Scientific Instruments*, *87*(2), 024502. https://doi.org/10.1063/1.4941960

Ogilvie, K. W., & Coplan, M. A. (1995). Solar wind composition. *Reviews of Geophysics*, *33*(1 S), 615–622. https://doi.org/10.1029/95RG00122

Orlando, T. M., Jones, B., Paty, C., Schaible, M. J., Reynolds, J. R., First, P. N., et al. (2018). Catalyst: Radiation effects on volatiles and exploration of asteroids and the lunar surface. *Chem*, *4*(1), 8–12. https://doi.org/10.1016/j.chempr.2017.12.004

Pabari, J., Nambiar, S., Shah, V., & Bhardwaj, A. (2020). Lunar regolith and water ice escape due to micrometeorite bombardment. *Icarus*, *338*, 113510. https://doi.org/10.1016/j.icarus.2019.113510

Paige, D. A., Siegler, M. A., Zhang, J. A., Hayne, P. O., Foote, E. J., Bennett, K. A., et al. (2010). Diviner lunar radiometer observations of cold traps in the Moon's south polar region. *Science*, *330*(6003), 479–482. https://doi.org/10.1126/science.1187726

Pieters, C. M., Goswami, J. N., Clark, R. N., Annadurai, M., Boardman, J., Buratti, B., et al. (2009). Character and spatial distribution of OH/H_2O on the surface of the Moon seen by M3 on Chandrayaan-1. *Science*, *326*(5952), 568–572. https://doi.org/10.1126/SCIENCE.1178658/SUPPL_FILE/PIETERS.SOM.PDF

Plimpton, S. J., & Thompson, A. P. (2012). Computational aspects of many-body potentials. *MRS Bulletin*, *37*(5), 513–521. https://doi.org/10.1557/mrs.2012.96

Pokorny, P., Mazarico, E., & Schorghofer, N. (2021). Erosion of volatiles by micrometeoroid bombardment on ceres and comparison to the Moon and mercury. *The Planetary Science Journal*, *2*(3), 85. https://doi.org/10.3847/PSJ/abef04

Poppe, A. R., Farrell, W. M., & Halekas, J. S. (2018). Formation timescales of amorphous rims on lunar grains derived from Artemis observations. *Journal of Geophysical Research: Planets*, *123*(1), 37–46. https://doi.org/10.1002/2017JE005426

qi Shen, R., shun Bai, Q., hai Li, Y., & hu Zhang, F. (2019). Molecular dynamics simulation of phase transformation of fused silica under nanoparticle impact: The influence of temperature and impact velocity. *Computational Materials Science*, *170*, 109169. https://doi.org/10.1016/j.commatsci.2019.109169

Rahnamoun, A., & van Duin, A. C. T. (2016). Study of ice cluster impacts on amorphous silica using the ReaxFF reactive force field molecular dynamics simulation method. *Journal of Applied Physics*, *119*(9), 095901. https://doi.org/10.1063/1.4942997

Samela, J., & Nordlund, K. (2010). Classical molecular dynamics simulations of hypervelocity nanoparticle impacts on amorphous silica. *Physical Review B: Condensed Matter*, *81*(5), 054108. https://doi.org/10.1103/PhysRevB.81.054108

Schaible, M. J., & Baragiola, R. A. (2014). Hydrogen implantation in silicates: The role of solar wind in SiOH bond formation on the surfaces of airless bodies in space. *Journal of Geophysical Research: Planets*, *119*(9), 2017–2028. https://doi.org/10.1002/2014JE004650

Schörghofer, N., Benna, M., Berezhnoy, A. A., Greenhagen, B., Jones, B. M., Li, S., et al. (2021). Water group exospheres and surface interactions on the Moon, Mercury, and Ceres, *217*(6), 74. https://doi.org/10.1007/s11214-021-00846-3

Sheikholeslam, S. A., Manzano, H., Grecu, C., & Ivanov, A. (2016). Reduced hydrogen diffusion in strained amorphous SiO_2: Understanding ageing in MOSFET devices. *Journal of Materials Chemistry C: Materials for Optical and Electronic Devices*, *4*(34), 8104–8110. https://doi.org/10.1039/C6TC02647H

Sorokin, E., Yakovlev, O., Slyuta, E., Gerasimov, M., Zaitsev, M., Shcherbakov, V., et al. (2020). Experimental modeling of a micrometeorite impact on the Moon. *Geochemistry International*, *58*(2), 113–127. https://doi.org/10.1134/S0016702920020111

Starukhina, L. (2006). Polar regions of the Moon as a potential repository of solar-wind-implanted gases. *Advances in Space Research*, *37*(1), 50–58. (The Moon and Near-Earth Objects). https://doi.org/10.1016/j.asr.2005.04.033

Stern, S. A., Cook, J. C., Chaufray, J. Y., Feldman, P. D., Gladstone, G. R., & Retherford, K. D. (2013). Lunar atmospheric H_2 detections by the LAMP UV spectrograph on the lunar reconnaissance orbiter. *Icarus*, *226*(2), 1210–1213. https://doi.org/10.1016/J.ICARUS.2013.07.011

Stukowski, A. (2009). Visualization and analysis of atomistic simulation data with OVITO–the open visualization tool. *Modelling and Simulation in Materials Science and Engineering*, *18*(1), 015012. https://doi.org/10.1088/0965-0393/18/1/015012

Sunshine, J. M., Farnham, T. L., Feaga, L. M., Groussin, O., Merlin, F., Milliken, R. E., & A'Hearn, M. F. (2009). Temporal and spatial variability of lunar hydration as observed by the deep impact spacecraft. *Science*, *326*(5952), 565–568. https://doi.org/10.1126/science.1179788

Verkercke, S., Chaufray, J.-Y., Leblanc, F., Bringa, E. M., Tramontina, D., Morrissey, L., & Woodson, A. (2023). Effects of airless bodies' regolith structures and of the solar wind's properties on the backscattered energetic neutral atoms flux. *The Planetary Science Journal*, *4*(10), 197. https://doi.org/10.3847/PSJ/acf6bd

Von Steiger, R., Schwadron, N. A., Fisk, L. A., Geiss, J., Gloeckler, G., Hefti, S., et al. (2000). Composition of quasi-stationary solar wind flows from Ulysses/solar wind ion composition spectrometer. *Journal of Geophysical Research*, *105*(A12), 27217–27238. https://doi.org/10.1029/1999JA000358

Williams, J.-P., Paige, D., Greenhagen, B., & Sefton-Nash, E. (2017). The global surface temperatures of the Moon as measured by the diviner lunar radiometer experiment. *Icarus*, *283*, 300–325. (Lunar Reconnaissance Orbiter - Part II). https://doi.org/10.1016/j.icarus.2016.08.012

Williams, R. J., & Jadwick, J. (1980). Handbook of lunar materials.

Wu, Y., Li, X., Yao, W., & Wang, S. (2017). Impact characteristics of different rocks in a pulsed laser irradiation experiment: Simulation of micrometeorite bombardment on the Moon. *Journal of Geophysical Research: Planets*, *122*(10), 1956–1967. https://doi.org/10.1002/2016JE005220

Zeller, E. J., Ronca, L. B., & Levy, P. W. (1966). Proton-induced hydroxyl formation on the lunar surface. *Journal of Geophysical Research*, *71*(20), 4855–4860. https://doi.org/10.1029/JZ071i020p04855

Zhu, C., Crandall, P. B., Gillis-Davis, J. J., Ishii, H. A., Bradley, J. P., Corley, L. M., & Kaiser, R. I. (2019). Untangling the formation and liberation of water in the lunar regolith. *Proceedings of the National Academy of Sciences of the United State of America*, *116*(23), 11165–11170. https://doi.org/10.1073/pnas.1819600116